Journal of Catalysis 316 (2014) 210–218

Contents lists available at ScienceDirect

Journal of Catalysis

journal homepage: www.elsevier.com/locate/jcat

Reversible deactivation of a $Au/Ce_{0.62}Zr_{0.38}O_2$ catalyst in CO oxidation: A systematic study of CO_2-triggered carbonate inhibition

Eloy del Río [a], Sebastián E. Collins [b,*], Alejo Aguirre [b], Xiaowei Chen [a], Juan Jose Delgado [a], Jose Juan Calvino [a], Serafín Bernal [a]

[a] Departamento de Ciencia de los Materiales, Ingeniería Metalúrgica y Química Inorgánica, Facultad de Ciencias, Universidad de Cádiz, Campus Río San Pedro, E-11510 Puerto Real (Cádiz), Spain
[b] Instituto de Desarrollo Tecnológico para la Industria Química (CONICET, UNL), Güemes, 3450, S3000GLN Santa Fe, Argentina

ARTICLE INFO

Article history:
Received 20 March 2014
Revised 19 May 2014
Accepted 20 May 2014

Keywords:
Gold catalyst
CO oxidation
Deactivation
Carbonate species
CO_2 poisoning
Mass spectrometry isotopic analysis
Time-resolved infrared spectroscopy
DRIFT
Modulation excitation spectroscopy (MES)
Reaction mechanism

ABSTRACT

Highly active supported gold catalysts frequently undergo substantial decrease in activity due to deactivation. The aim of this paper is to investigate a reversible inhibition phenomenon of the CO oxidation in an $Au/Ce_{0.62}Zr_{0.38}O_2$ (Au/CZ) catalyst. The results of a systematic study of CO oxidation conditions (CO, O_2, and CO_2) are discussed. By identifying CO_2 as an Au/CZ poison using isotopic transient analysis ($^{13}CO/^{12}CO_2$), we also investigate the origin of inhibition activity by transient and modulated infrared spectroscopy in DRIFT mode. Results demonstrate that carbonate species are formed by reaction of CO_2 with reactive lattice oxygen at the metal–support interphase, which in turn inhibits the replenishment of the vacancies by molecular oxygen. A microkinetic model that accounts for the reaction mechanism and inhibition by CO_2 is proposed.

© 2014 Elsevier Inc. All rights reserved.

1. Introduction

Gold-supported catalysts present outstanding performance in oxidation reactions [1,2], such as CO oxidation [3,4], PROX (selective oxidation of CO in presence of an excess of H_2) [5,6], low-temperature water gas shift [7,8], and combustion of volatile organic compounds [9]. Many works have been devoted to understand mechanisms by which these catalysts carry out oxidation reactions. This is a key step to design improved catalytic materials. Particularly, low-temperature CO oxidation has been taken as a prototypical catalytic reaction by gold [2,10–15]. According to Haruta's classical mechanism, previously reported over Au/TiO_2 catalysts [16], CO rapidly adsorbs on low-coordination surface Au sites, and it is oxidized at the perimeter of metal nano-particles where oxygen is activated [13]. Also recently, Yates et al. [14] proposed the existence of a dual mechanism at the perimeter zone of reactivity between CO adsorbed on Au and TiO_2 for very low-temperature CO oxidation. However, despite the apparent simplicity of the catalytic oxidation of CO on gold-supported catalysts, some aspects of the reaction mechanism still remain unclear, particularly those regarding with the deactivation process. Actually, a major drawback of Au catalysts is their severe deactivation. This undesirable phenomenon, frequently observed on those materials, has reduced their potential for industrial applications [17–19]. Among other causes, deactivation has been reported to be due to: (1) sintering of supported Au nano-particles [4,20,21]; (2) changes in the oxidation state of the Au sites [10,22,23]; (3) loss of the metal–support interaction [19,24]; and (4) poisoning by carbonate-like species [10,18,21,23,25–28]. Other factors such as chloride content [15,29] or moisture level from the gaseous mixture [12,30] have also occasionally been regarded as poisons (or even as a promoter in the case of H_2O), something which puzzles a full understanding of the origin of the inhibition mechanism.

Although gold supported on ceria or ceria-based support catalysts have been widely studied, there have been very few studies focused on the mechanism of their deactivation, and especially their eventual regeneration [3,8,19,31]. In this work, the catalytic stability of a well-characterized $Au/Ce_{0.62}Zr_{0.38}O_2$ catalyst [4,32–35] is studied in detail, particularly aiming at understanding the reversible loss of reaction rate observed between the heating and cooling branches of light-off experiments. The structural

* Corresponding author.
E-mail address: scollins@santafe-conicet.gov.ar (S.E. Collins).

http://dx.doi.org/10.1016/j.jcat.2014.05.016
0021-9517/© 2014 Elsevier Inc. All rights reserved.

stability of the catalyst is investigated by X-ray diffraction, (Scanning)-Transmission Electron microscopy and X-ray photoelectronic spectroscopy (XPS). The role of reactants, products and moisture is studied by online mass spectrometry using isotopic transient analysis ($^{13}CO/^{12}CO_2$) and infrared spectroscopic techniques. Particularly, diffuse reflectance infrared spectroscopy (DRIFT) in time-resolved and concentration-modulation excitation spectroscopy (c-MES) modes was employed to gain a molecular view of the catalytic inhibition produced by adsorbed surface species. Moreover, a comprehensive microkinetic model that accounts for the reaction mechanism and inhibition by CO_2 is proposed.

2. Experimental

The gold catalyst with a 2.6 wt% metal loading was prepared by a deposition–precipitation with urea using $H[AuCl_4]$ (Alfa Aesar, 99.99%) as Au precursor [32]. The mixed oxide support, $Ce_{0.62}Zr_{0.38}O_2$ (S_{BET} = 68 $m^2\ g^{-1}$), was kindly donated by Grace Davison. The fresh catalyst was submitted to an activation protocol consisting in heating under flow of O_2(5%)/He (10 K min^{-1}) from 298 K to 523 K (1 h), followed by purging with pure He at 523 K (1 h), and then cooled to 298 K, under flowing He. This activated catalyst sample, with a surface area of 63 $m^2\ g^{-1}$ will be hereafter referred to as Au/CZ.

The metal dispersion was determined by high-resolution electron transmission microscopy (HRTEM) and scanning transmission electron microscopy high-angle annular dark field (STEM-HAADF) techniques [35]. HAADF-STEM images were obtained on a JEOL2010F instrument using a 0.5 nm electron probe at a camera length of 10 cm. This STEM-HAADF imaging mode provides contrasts directly related to the average atomic number (Z) in the region under the electron beam. In any case, the nature of the particles included in the size distribution was further confirmed by X-ray energy dispersive spectroscopy in STEM mode.

X-ray photoelectron spectroscopy studies were performed on a Kratos Axis Ultra DLD instrument equipped with a catalytic cell allowing a clean transfer of the pretreated samples to the analytical chamber. Spectra were recorded by using monochromatized Al Kα radiation [4]. X-ray diffraction studies were performed on a Bruker D8 Advance equipment. Diffraction patters were acquired using Cu Kα radiation, in the 2θ 5–85° range, with a 0.05° step and a recording time of 30 s per step.

Catalytic assays were performed under the following conditions: 25 mg of catalyst diluted with 100 mg of crushed quartz were place in a tubular quartz reactor (i.d. = 4 mm) and the gas flow was adjusted to a reaction mixture consisting of 1% CO, 0.6% O_2, and He to balance was 100 ml min^{-1} by means of gas flow controllers. The reactor was immersed in a bath Lauda, model Proline RP-845, filled with polymethylsiloxane, whose temperature could be varied with excellent linearity within the range 233–418 K, and heating/cooling rate: 10 K min^{-1}. The gas composition at the reactor exit was continuously monitored by a quadrupole mass spectrometer (MS), Pfeiffer Vacuum Prisma, model QME-200-D. Prior to running the activity assays, the catalyst samples were activated in situ as described before.

Diffuse reflectance infrared spectroscopy (DRIFT) experiments were carried out using a high-temperature reaction cell (Harrick) fitted with KBr windows. The reaction flow was going down through the reactor bed, so that the upper layer of the catalyst, approximately 200 μm, is probed by IR beam in the front of the bed. The amount of catalyst used in the DRIFTS cell was 25 mg, with a bed height of about 5–7 mm. The cell was connected to the feed gas cylinders through low-volume stainless-steel lines. Rapid exchange of the gas composition was performed by switching an electronically actuated flow-through valve (Vici-Valco Instruments) which avoided pressure drops during changes, synchronized with the FTIR spectrometer. The gas flows were adjusted by mass flow controllers. The DRIFT cell was mounted inside the sample compartment of the FTIR spectrometer (Thermo-Electron, Nicolet 8700 with a cryogenic MCT detector). The bench of the spectrometer was continuously purged with dried air (Parker Balston FTIR purge gas generator) to eliminate CO_2 and water vapor contributions to the spectra. Time-domain IR spectra were recorded in kinetic and rapid-scan mode at a resolution of 4 cm^{-1}. The reference spectrum was collected without catalyst.

Concentration-modulation excitation spectroscopy (c-MES) experiments were performed using the set up described elsewhere [36]. After recording the background spectrum, a modulation experiment was started by varying the inlet mass flow of the reaction gas using the desired modulation frequency. After waiting at least five modulation periods to allow for an adjustment of the system to the external perturbation, the recording of the spectra was started. At least 125 spectra in each c-MES period were acquired, using reactant exchange frequencies from 1.7 to 33 mHz. Phase-sensitive detection (PSD) analysis of the spectra was performed according to the method developed by Baurecht and Fringeli [37].

3. Results

3.1. Studies of catalytic activity by Mass Spectrometry (MS)

Fig. 1(a) shows the light-off traces during CO oxidation on Au/CZ catalyst through two consecutive heating–cooling cycles.

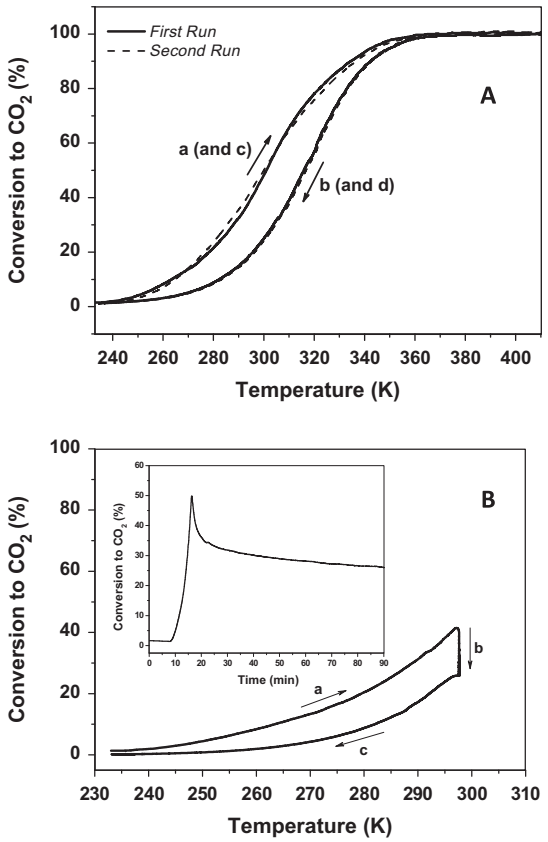

Fig. 1. (A) CO oxidation activity on Au/CZ catalyst: first run (solid line) and second run (dashed line) (a and c heating, and b and d cooling parts of the essay). Reaction mixture: 1% CO, 0.6% O_2 in He, 100 ml min^{-1}, heating and cooling ramps: 10 K min^{-1}. (B) Conversion–temperature curves corresponding to the following sequence: (a) heating from 233 K to 298 K (10 K min^{-1}), (b) isothermal step at 298 K for 30 min, and (c) cooling from 298 K to 233 K. Inset shows the time evolution of the CO_2 trace at 298 K (stage b).

As deduced from that figure, during the heating step, the catalyst presents a steep increase in the conversion of CO, with a T_{50} (50% of CO conversion) at 295 K and reaches total conversion at 353 K. However, the activity of the catalyst during the cooling step is lower than that exhibited throughout the heating one. As shown in the figure, this behavior is completely reversible during consecutive cycles. In fact, the light-off curves are completely superimposable in both heating and cooling branches. In order to clarify the influence of temperature, Fig. 1(b) shows an additional experiment carried out under reaction conditions from 233 K to 298 K followed by an isotherm stage at 298 K for 30 min, and finally cooling from 298 K to 233 K (-10 K min^{-1}). Interestingly, a similar deactivation effect of hysteresis loop is observed at room temperature with a significant drop in CO conversion, which decreases from 45% to 25% at 298 K.

A detailed characterization of the activated and post-reaction Au/CZ catalysts was carried out in order to detect structural changes that could account for the observed deactivation. HRTEM, XRD and XPS investigation revealed that the gold particle size distribution and their oxidation state remained constant after the reaction cycles. This was also the case for the texture and crystalline structure of the support (see Supplementary Information for details). From these results, it is concluded that the highly dispersed gold nanoparticles do not sinter while increasing the reaction temperature.

Altogether, these results point to a reversible deactivation or inhibition of the oxidation of CO on the Au/CZ catalyst. Hence, in order to further investigate the possible chemical origin of this reversible inhibition of the catalyst activity, a series of systematic reaction test were performed using combination of reactants and purge cycles.

Fig. 2 presents the MS traces after switching back and forward from a reaction CO+O_2 mixture to pure He at 308 K. The analysis of the reaction transient shows a peak of CO oxidation at the beginning of the reactant contact with the catalyst, and a progressive decay in the CO conversion until a pseudo-steady-state condition is reached. Then, the initial reaction activity can be completely restored by flowing pure He for 15 min at 308 K. the effect of sweep time under inert gas flow was studied at 308 K (see Supporting Information for details). In particular, the sweep time was reduced from 15 min to 5 min, and 1 min. As can be seen in Fig. S4, 5 min is enough time to produce the same degree of regeneration. However, when the sweep time is reduced to 1 min, the achieved regeneration level, although noticeable, is significantly lower.

Considering these results, the role of adsorbed oxygen was firstly studied. Recently, Yates and co-workers reported a 22-fold lower CO oxidation activity over a pre-oxidized Au/TiO_2 catalyst, a result which they attributed to oxygen chemisorbed on gold sites with partial positive charge [15]. In clear contrast, the results recorded after pre-adsorbing oxygen on our Au/CZ catalyst at 308 K (10 min) and exposing it again to the reaction mixture shows a more intense transient of CO_2 production (Fig. 3). Complementary experiments allowed us to conclude that oxygen has a positive reaction order. Therefore, we can rule out an oxygen inhibition of the CO oxidation over the Au/CZ catalyst.

Similar experiments were performed to investigate a possible inhibition by CO, either by over-reduction of the support (e.g. at the particle/support interface) [33] or by forming adsorbed carbonates species [34] that could block the reaction pathway. Nevertheless, the reaction transient was almost identical after purging with He or pre-reacting the catalyst under a flow of CO (Fig. 4). Additional experiments were performed varying the CO partial pressure in the reaction feed, from 1% to 5% of CO while maintaining the constant the CO/O_2 ratio, and similar profiles of the conversion were obtained. Therefore, these observations strongly support that the loss of catalytic activity is not correlated with a self-inhibition provoked by CO.

It has been reported that even traces of water can influence the activity of supported gold catalysts [3,12,30]. A complementary experiment was carried out by passing the reactants by a liquid-N_2 cold trap to eliminate traces of moisture. It is worth mentioning that this cold trap was used throughout the experiment, including the previous stage of catalyst activation. According to Fig. S5, the conversion–time transient presents the usual profile and the activity decays during the period in which the reactor is fed with CO and O_2, and partially regenerated after flowing pure He. Thus, we can rule out the influence of traces of moisture on the deactivation in this case.

The effect of the concentration of CO_2 was also investigated. In order to be able to separate signals of CO_2 produced by the reaction from that of the feed, isotopically labeled reactants were employed. Fig. 5(a) shows that after pre-exposing the catalyst to (1%)$^{12}CO_2$ at 308 K, the initial ^{13}CO oxidation peak disappeared, but that it can be restored by simply purging with helium. These data clearly indicate that when the catalyst is in contact with the gas stream containing 1% of $^{12}CO_2$, the conversion–time curve is nearly flat. Interestingly, this experiment suggests that weakly adsorbed CO_2 forms on the catalyst may contribute to the effect of poisoning that occurs during the catalytic reaction. Moreover,

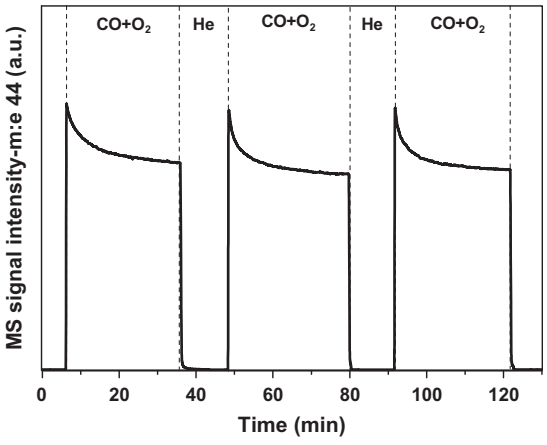

Fig. 2. Isothermal CO oxidation (1% CO, 0.6% O_2 in He, 100 ml min^{-1}) at 308 K on the Au/CZ catalyst as a function of consecutive switching from pure He (60 ml min^{-1}, 15 min) to the reaction mixture (30 min).

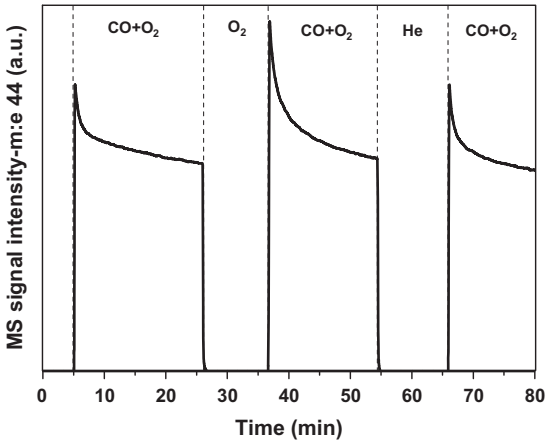

Fig. 3. Isothermal CO oxidation (1% CO, 0.6% O_2 in He, 100 ml min^{-1}) at 308 K on the Au/CZ catalyst as a function of consecutive switching from pure O_2 (60 ml min^{-1}, 15 min) and after purge with pure He (60 ml min^{-1}, 15 min).

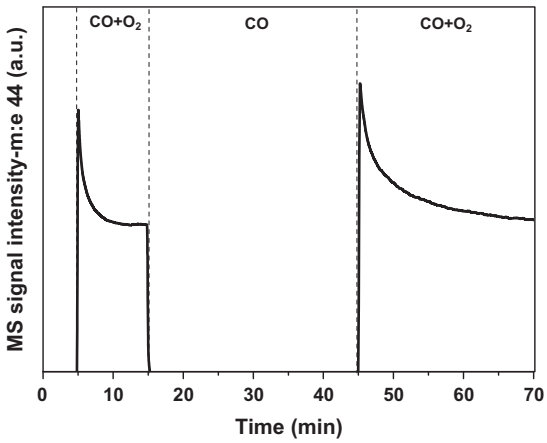

Fig. 4. Isothermal CO oxidation (1% CO, 0.6% O_2 in He, 100 ml min^{-1}) at 308 K on the Au/CZ catalyst after exposure to (1%)CO/He (60 ml min^{-1}, 15 min) and after purging with pure He (60 ml min^{-1}, 15 min).

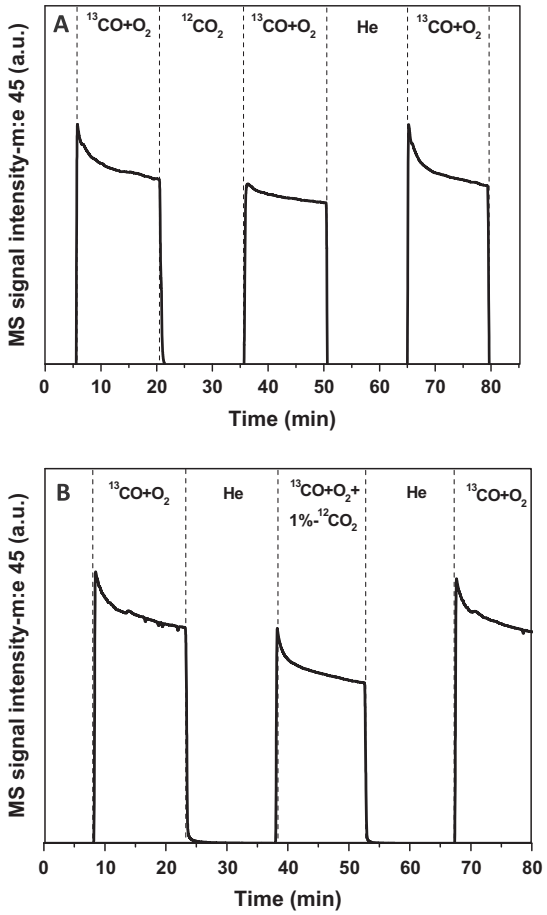

Fig. 5. (A) Evolution of the MS signal of $^{13}CO_2$ (m/e = 45) after consecutive switching of: (i) reaction mixture (1% ^{13}CO, 0.6% O_2 in He, 100 ml min^{-1}), (ii) (1%)$^{12}CO_2$ /He (15 min, 60 ml min^{-1}), (iii) pure He (15 min, 60 ml min^{-1}), over the Au/CZ catalyst at 308 K. (B) Effect of the co-feeding of $^{12}CO_2$ in the reaction mixture (1% ^{13}CO, 1% $^{12}CO_2$, 0.6% O_2 in He, 100 ml min^{-1}) in consecutive cycles of reaction and purge with pure He.

when (1%)$^{12}CO_2$ is co-feed with the reaction mixture of $^{13}CO+O_2$, a strong inhibition of the activity was verified. Again, the initial activity can be fully recovered by simply purging with He, Fig. 5(b).

A further confirmation of the inhibitory effect of CO_2 was obtained by carrying out two consecutive light-off cycles; a first one in which only CO and O_2 were used as reactants followed by a second one in which CO_2 was co-fed with these reactants. Results included in Fig. 6 show that the traces of carbon dioxide produced by the reaction in the presence of $^{13}CO_2$ are significantly shifted to higher temperature values with respect to those observed for the catalytic test ran under the conventional reaction conditions (CO and O_2). Since carbon monoxide oxidation is such an exothermic (irreversible) reaction, we can conclude that CO_2 is inhibiting some step of the reaction mechanism as will be discussed next.

3.2. Time-resolved in situ DRIFT spectroscopy: Transient oxidation of CO species

To gain direct information about the origin of the CO_2 inhibition on the Au/CZ catalyst, experiments using time-resolved infrared spectroscopy in DRIFT mode were performed. Fig. 7A presents DRIFT spectra (1 spectrum/0.39 s) collected after switching the gas flow from (1%)CO/He to (0.6%)O_2/He at 308 K. Under steady-state flow of (1%)CO into the cell (t = 0 s), a series of signals due to CO adsorbed on gold are present at 2107, 2060 and 2015 cm^{-1} (Note that bands due to the P and R branch of CO in the gas phase were carefully subtracted in these spectra for clarity.). Those spectral features can be assigned as follows: the absorption band around 2110 cm^{-1} is typical of the stretching mode of CO, ν(CO), linearly chemisorbed on metallic gold sites, Au^0 [32,38,39]; on the other hand, bands below 2100 cm^{-1} can be assigned to CO adsorbed on negatively charged gold clusters, $Au^{\delta-}$ [40,41]. Such a downward shift of the frequency may be explained by the back donation from Au to the $2\pi^*$ antibonding orbital of CO [42,43]. Fielicke et al. [44] found an approximately linear relationship between the red-shift of the vibrational spectra of CO adsorbed on negatively charged gold clusters and the density of charge in the cluster, e.g. $Au_n(CO)_m^-$ (m, $n < 14$) shifts from 2062 cm^{-1} for the n = 2 cluster to 1995 cm^{-1} for the n = 14 cluster. The origin of negatively charged gold sites on supported gold catalysts have been interpreted as a charge transfer from the color centers (oxygen vacancies) on the oxide surface to the gold clusters. The electron transfer from partially reduced oxides, such as TiO_2 or MgO to atoms, to gold clusters or films has been corroborated both experimentally and theoretically [41–43]. The stability of the catalyst after several cycles of CO oxidation seems to indicate that the small gold clusters, where negatively gold sites would be located, are stable too. These gold clusters could be stabilized at support

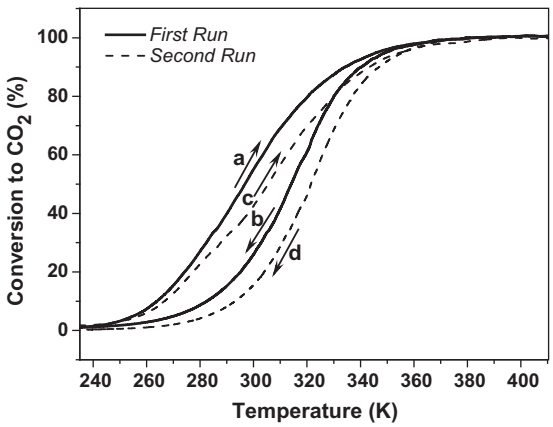

Fig. 6. CO oxidation activity on Au/CZ catalyst for two full consecutive tests (heating and cooling). In the first run (solid line, a and b), the reaction mixture was: ^{13}CO(1%) and O_2(0.6%) in He, 100 ml min^{-1}; in the second run (dash line, c and d) was: ^{13}CO(1%), O_2(0.6%) and $^{12}CO_2$ (1%) in He, 100 ml min^{-1}. Heating and cooling ramps: 10 K min^{-1}.

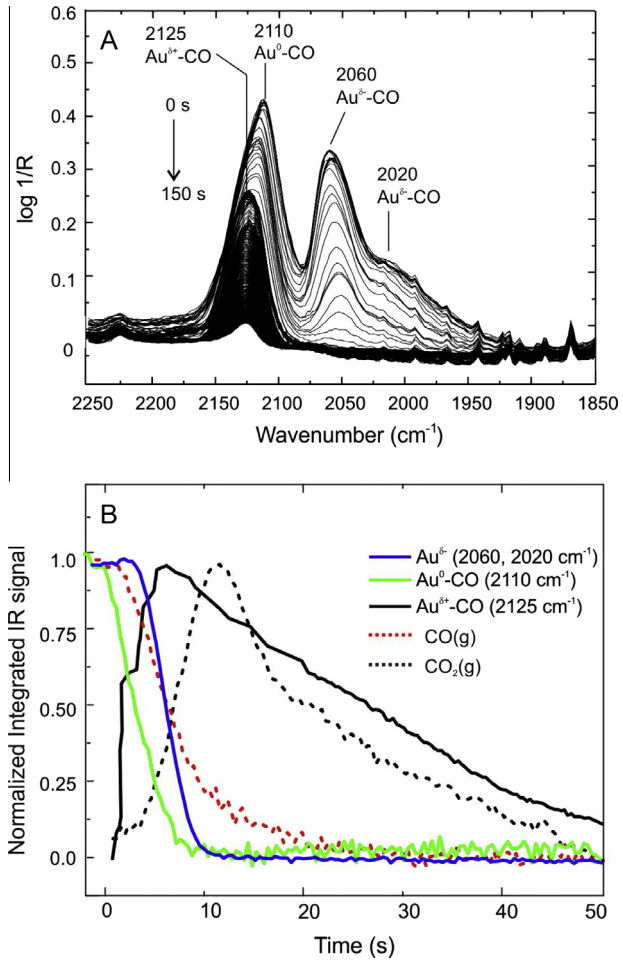

Fig. 7. (A) Time-resolved DRIFT spectra (1 spectrum/0.39 s) collected after switching the gas flow from (1%)CO/He ($t = 0$) to (0.6%)O_2/He (308 K). Total gas flow: 100 ml min^{-1}. (B) Time-evolution of selected infrared signals.

defect, steps and corners, as was observed by using 3D HAADF-STEM Electron Tomography in a similar system [45].

After switching the gas flow from (1%)CO to (0.6%)O_2, the evolution of the infrared spectra shows that the low frequency bands are rapidly consumed and CO_2(g) is produced (bands around 2350 cm^{-1}, not shown), while the absorption band at 2110 cm^{-1} decreases and a new overlapped band at 2125 cm^{-1} shows up and then slowly decreased. The time-evolution of each overlapped band was followed, after deconvolution using a sum of Lorentz functions, and the corresponding integrated absorbance is presented in Fig. 7B as a measurement of the amount of the corresponding species on the surface and gas phase. Bands at 2060 and 2020 cm^{-1} decrease at the same time that CO_2(g) is produced and CO(g) is swept from the cell. Meanwhile, a rapid consumption of the absorption band at 2110 cm^{-1} is observed at the same time that the band at 2125 cm^{-1} increases its intensity, reaching a maximum at 6 s, and then slowly decreased. Note that when switching from CO/He to pure He, no shift in the signal at 2110 cm^{-1} is observed (spectra not shown). The band at 2125 cm^{-1} is generally assigned to CO adsorbed on positively charged Au$^{\delta+}$ sites ($0 < \delta < 1$) [44]. Boccuzzi and co-workers have also ascribed this band to the interaction of adsorbed oxygen and CO on gold particles, Au$^{\delta+}$–CO [39,46–48]. Very recently, Yates and co-workers [14,15], using infrared measurements and DFT calculations, assigned a band at 2126 cm^{-1} on pre-oxidized Au/TiO_2 to CO adsorbed on Au$^{\delta+}$ ($\delta = 0.1$–0.3) with O adatoms that inductively increase the positive charge of Au atoms in gold particles. Also, calculation shows that this positive charge directly influence the vibrational frequency of CO adsorbed on these electropositive Au sites in +14–23 cm^{-1}, in excellent agreement with the +20 cm^{-1} blue shift observed experimentally (from ~2106 to ~2126 cm^{-1}). Moreover, these authors showed that bands at 2126 and 2110 cm^{-1} can be interconverted as a result of the adsorption or desorption of O adatoms.

Following the evolution of the integrated bands at 2110 and 2125 cm^{-1}, Au^0–CO and Au$^{\delta+}$–CO, respectively, it is observed that the first signal decays at the same rate than the second is formed, e.g. $t < 5$ s, but without CO_2(g) production. This result points to an interconversion of both bands due to the positive charge acquired by the gold site during O_2 chemisorption [14,15]. Then, Au$^{\delta+}$–CO slowly reacted decaying in ca. 100 s. Thus, we can conclude that CO adsorbed on negatively charged clusters (2060 and 2020 cm^{-1}) are the most reactive adsorbed species, while CO adsorbed on positively charged gold sites showed much slower reactivity. Consistent with this picture, during steady-state CO + O_2 reaction monitored by DRIFT, only a band at 2125 cm^{-1} was registered. After switching from reaction mixture to (0.6%)O_2/He, that band took ca. 70 s to be consumed (spectra not shown).

In a similar manner, the effect of CO_2 on the reactivity of CO bonded species was studied in a series of transient experiments followed by DRIFT, exchanging (1%)CO + (1%)CO_2/He to (0.6%)O_2 + (1%)CO_2/He in the temperature range of 293–323 K. In Fig. 8 the evolution of both bands at 2060 and 2020 cm^{-1}, without and with CO_2 are compared. Thus, a slight delay in the rate of Au$^{\delta-}$–CO oxidation is observed when CO_2 was co-fed. In turn, the evolution of Au^0–CO and Au$^{\delta+}$–CO species is shown in Fig. 9A and B (at 308 K). As observed in the figure, the presence of CO_2(g) does not affect the conversion of Au–CO (2110 cm^{-1}) to Au$^{\delta+}$–CO (2125 cm^{-1}), $t < 5$ s, but a strong lag in the consumption of Au$^{\delta+}$–CO is registered when CO_2 was co-fed.

3.3. Role of the carbonate-adsorbed species: modulation excitation spectroscopy (c-MES)

As shown before, the presence of CO_2 in the gas phase clearly seems to inhibit some part of the CO oxidation mechanism in our Au/CZ catalyst. It is well known that ceria–zirconia mixed oxides adsorb CO_2 forming a variety of surface (and also bulk) carbonate species [32].

DRIFT spectra collected under steady-state CO oxidation and from transient time-resolved (e.g. CO to O_2) present a strong background in the carbonate region (1800–1000 cm^{-1}). Thus, it is

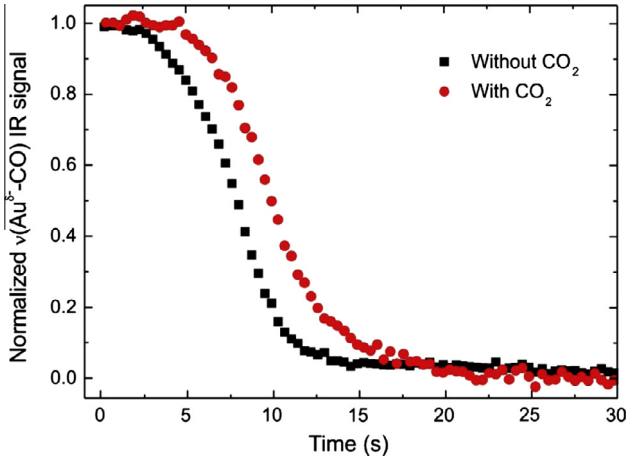

Fig. 8. Evolution of the Au$^{\delta-}$–CO signals (2060 and 2020 cm^{-1}) after switching the gas flow from (1%)CO/He ($t = 0$) to (0.6%)O_2/He at 308 K without and with (1%)CO_2.

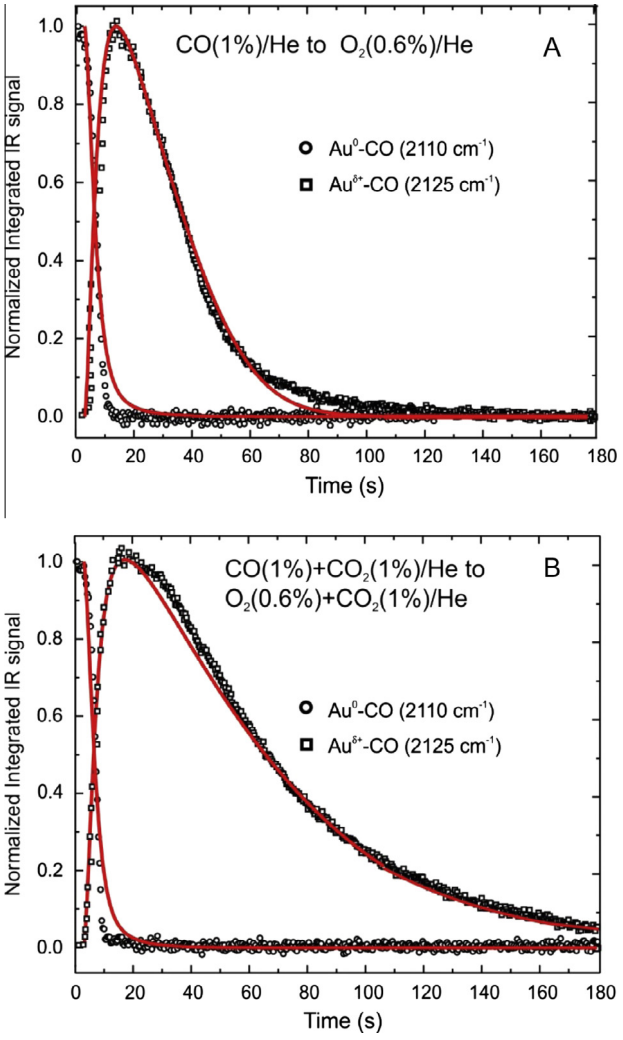

Fig. 9. Evolution of Au^0–CO and $Au^{\delta+}$–CO signals after switching the gas flow from (1%)CO/He ($t = 0$) to (0.6%)O_2/He (100 ml min^{-1}, 308 K, at 308 K without (A) and with (1%)CO_2 (B). Solid lines show the best fitting of the data using the model described in the text.

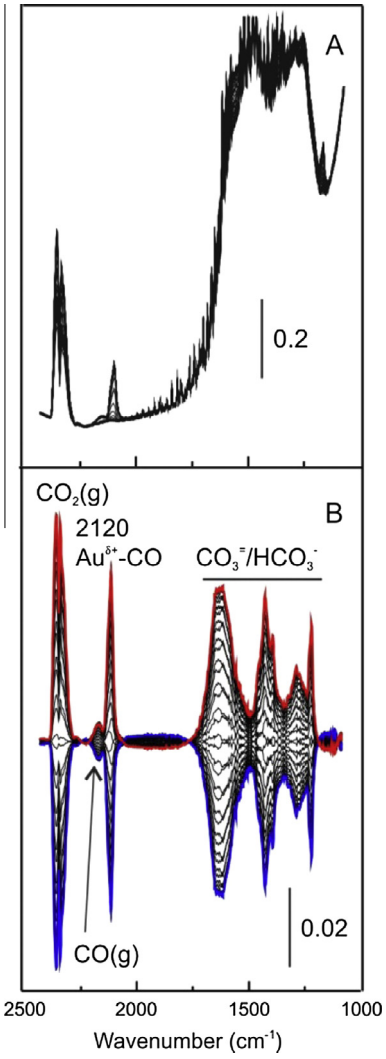

Fig. 10. (A) Time-domain DRIFT spectra during a c-MES cycle (1%)CO/He to (1%)O_2/He over Au/CZ (100 ml min^{-1}, 308 K, $\omega = 4.2$ mHz). (B) And phase-domain spectra after PSD demodulation.

difficult to obtain direct insights concerning to the surface groups (reversible and irreversible adsorption) that could be related to the deactivation observed in the Au/CZ catalyst. For that reason, we carried out c-MES experiments followed by DRIFT, exchanging periodically (1%)CO + (0.6%)O_2/He to He or (1%)CO + (0.6%)O_2 + CO_2(1%)/He to CO_2(1%)/He over the Au/CZ-OE523 catalyst at 308 K. Figs. 10 and 11 show the time-domain and phase-domain spectra (after PSD treatment) for each experiment. As seen in the figures, changes in the time-resolved spectra are observed in the Au–CO region and also in the CO_2 (g) signal; however, it is impossible in practice to obtain reliable information from the carbonate region (1800–1000 cm^{-1}). However, in the phase-domain spectra – after PSD demodulation – the evolution of the signals due to carbonate groups can be easily followed. The signals, which are affected by the applied perturbation, are assigned to the following carbonate species: bicarbonates, HCO_3^-, $\nu_{as}(CO_3) = 1640$ cm^{-1}, $\nu_s(CO_3) = 1433$ cm^{-1}, and $\delta(OH) = 1220$ cm^{-1}; bidentate carbonates, b-$CO_3^=$, $\nu_{as}(CO_3) = 1576$ cm^{-1} and $\nu_s(CO_3) = 1285$ cm^{-1}, and polydentate carbonates, and monodentate carbonate, m-$CO_3^=$, $\nu_{as}(CO_3) = 1393$ cm^{-1} [49–54]. Note the very low intensity of these bands, in the phase-domain, as compared to the whole set of bands in the carbonate region in the time-domain spectra. That means that only a minor part of the whole set of carbonate groups is reversibly adsorbed, and most of carbonate are spectators of the reaction. Bands in identical position were observed in complementary experiments exchanging CO to O_2 in Au/CZ and after modulated adsorption of 1%CO_2/He on the $CeZrO_2$ bare support. From these results, it is now clear that the reversible adsorption of CO_2 produces HCO_3^- and b- and m-$CO_3^=$ on the surface of the ceria–zirconia support, which infrared could reveal after c-MES DRIFT experiments.

4. Discussion

The reaction tests using transient experiments followed by mass spectrometry showed that a repetitive hysteresis loop is obtained when CO is oxidized in heating and cooling ramps on an Au/CZ catalyst (Fig. 1). However, although the effect of the deactivation of gold catalysts on the CO oxidation reaction has been studied in the recent past, very few studies have focused on hysteresis loop phenomena [20,55]. Additionally, transient investigation of the reaction at isothermal conditions showed a high initial activity after exposing the catalyst to CO + O_2, followed by a progressive loss of catalytic activity (Fig. 2). This initial peak was not observed when pre-exposing the catalyst to 1%CO_2 and a lower activity was also registered when co-feeding CO_2 in the reaction mixture

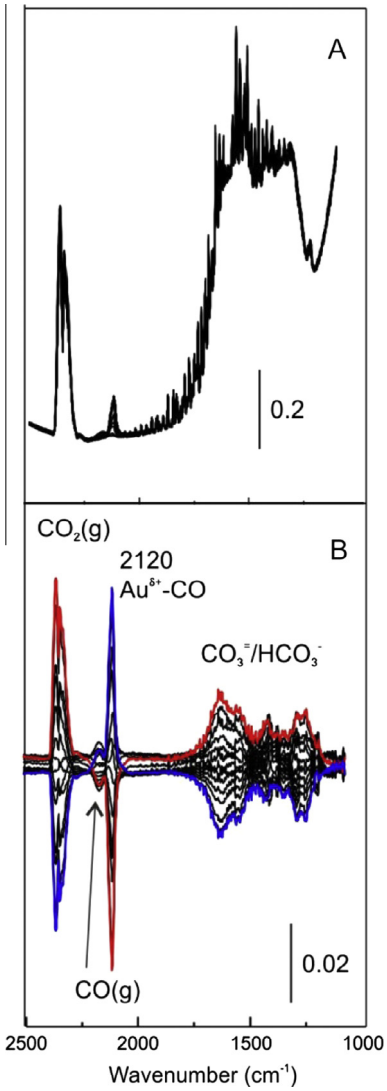

Fig. 11. (A) Time-domain DRIFT spectra during a c-MES cycle (1%)CO, (1%)CO_2 in He to (1%)O_2, (1%)CO_2 in He over Au/CZ (100 ml min^{-1}, 308 K, ω = 4.2 mHz). (B) Phase-domain spectra after PSD demodulation.

(Figs. 5 and 6). Moreover, the high initial activity of the catalyst was restored after purging with helium. Neither structural or textural changes nor an inhibition by CO, O_2 or H_2O were observed. All these results point out a product (CO_2) inhibition of the CO oxidation on this gold catalyst.

Transient time-resolved DRIFT experiments allowed to follow the evolution of CO-adsorbed species on gold after exchange of the gas stream from CO/He to O_2/He (Fig. 7). CO adsorbed on partially negatively charged gold clusters (bands <2000 cm^{-1}) were oxidized in ca. 10 s, but the consumption profile was retarded when CO_2 was present in the gas phase (Fig. 8). The most intense band at 2110 cm^{-1}, assigned to CO adsorbed on metallic gold sites, was observed to shift to 2125 cm^{-1} upon exposure to O_2. That is interpreted as a result of the co-adsorption of oxygen on the gold particles, which change gold to a more oxidized stated ($Au^{\delta+}$) making stronger the Au–CO bond. Then, the most stable $Au^{\delta+}$–CO species are oxidized to CO_2 in around 100 s, and moreover this process was significantly affected by the co-feeding of CO_2 (Fig. 9). Thus, we may conclude from those results that CO_2 is affecting part of the CO oxidation mechanism, particularly, the oxidation of the less-reactive CO adsorbed on positive gold.

Also, our c-MES experiments confirmed that most of the carbonate species bonded to the ceria–zirconia support are spectators of the reaction, but a very minor amount can be reversibly adsorbed. We identified this species as $HCO_3^{=}$, b- and m-$CO_3^{=}$. The evolution of the band of these groups is in correlation with the concentration of CO_2 in the gas phase. Furthermore, the variation in the amplitude of these signals is lower when CO_2 is co-fed along with CO or O_2. This means that more carbonate groups remain adsorbed when a higher partial pressure of CO_2 is present in the reaction mixture. This poisoning effect by CO_2 was shown to affect the reaction activity.

On Au/TiO_2, Overbury and co-workers [26,28] proposed that the CO_2 product can desorb from Au nanoparticles and re-adsorb in the support to form transient carbonate species which then slowly decompose to CO_2. This readsorption–decomposition process results in the slow evolution of CO_2 during this reaction compared to other components for this reaction. They interpret this result by proposing that the slow desorption of CO_2 from the support is the rate-limiting step in CO oxidation over Au/TiO_2 catalyst. In contrast, our transient analysis showed that CO_2 is rapidly produced at the beginning, after the surface was cleaned, and also that it is inhibited when CO_2 is co-fed in the reactor, that is when the support has a higher coverage of carbonate groups. Then, CO_2 should be interfering with another part of the reaction mechanism.

The special role of metal–support interfacial sites in ceria-based catalysts is under detailed investigation at present [56]. As it was reported by several authors [1,10,13,16,57], the gold-support perimeter is essential for the high activity shown by gold catalysts. Likewise, the oxidation of CO by lattice oxygen has been regarded as responsible of the activity in gold supported on reducible oxides, such as TiO_2, CeO_2, Fe_2O_3 [11,58,59]. Then, it is possible that the same lattice oxygen capable of oxidizing Au–CO can react with CO_2 forming carbonate groups. Then, this competitive adsorption of CO_2 could inhibit the oxidation reaction at Au–ceria–zirconia interphase sites.

4.1. CO_2 inhibition model

On gold supported on reducible metal oxides (e.g. TiO_2, CeO_2, $CeZrO_2$, among others), CO is proposed to adsorb on low-coordination surface Au sites, and to be oxidized by oxygen activated at the perimeter of the Au nanoparticles [13,16,57].

The results obtained by MS and in situ DRIFT spectroscopy allow us to propose the following reaction steps for the CO oxidation and partial inhibition by adsorbed CO_2 (summarized in Scheme 1):

(i) Adsorption of CO neutral and negatively charged clusters gold sites:

$$CO(g) + Au^0 \leftrightarrow Au^0{-}CO\ (2110\ cm^{-1})$$
$$CO(g) + Au^{\delta-} \leftrightarrow Au^{\delta-}{-}CO\ (2060\ \text{and}\ 2020\ cm^{-1})$$

(ii) Fast oxidation of CO on negatively charged clusters by lattice oxygen in the particle–support interface:

$$Au^{\delta-}{-}CO + O{-}S \leftrightarrow CO_2(g) + Au^{\delta-} + \text{v-S}\ (\text{v}: \text{O vacancy})$$

(iii) Adsorption of O_2 on gold particles and change in the oxidation state of gold sites:

$$1/2O_2(g) + Au^0{-}CO\ (2110\ cm^{-1})$$
$$\leftrightarrow (O)Au^{\delta+}{-}CO\ (2125\ cm^{-1})$$

(iv) Slow oxidation of CO in the particle–support interface

$$Au^{\delta+}{-}CO + O{-}S \leftrightarrow CO_2(g) + \text{v-S}$$

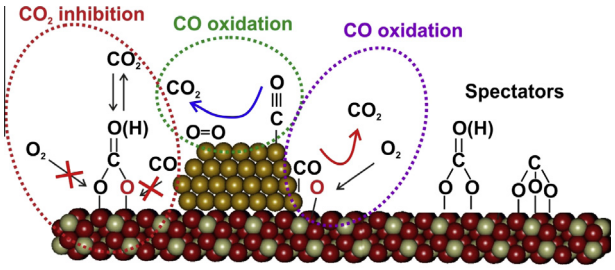

Scheme 1. Scheme of the proposed mechanism of CO oxidation and for the reversible deactivation produced by adsorbed carbonate species on the Au/CZ catalyst.

(v) Activation of O_2 in support sites (S) at the particle–support interface:

$$1/2O_2(g) + S \leftrightarrow O{-}S \text{ (slow)}$$

(vi) Adsorption of CO_2 to form carbonate species on the support sites:

$$CO_2(g) + O{-}S \leftrightarrow CO_3^{=}{-}S \text{ (fast)}$$

The above reaction mechanism is described by the following differential equations (see Supporting Information for details):

Step (i):

$$r_1 = k_1[CO(g)]\Gamma_{Au^0} - k_{-1}\Gamma_{Au^0-CO}$$
$$r_2 = k_2[CO(g)]\Gamma_{Au^{\delta-}} - k_{-2}\Gamma_{Au^{\delta-}-CO}$$

Step (ii):

$$r_{s1} = k_{s1}\Gamma_{Au^{\delta-}-CO}\Gamma_{O-S}$$

Step (iii):

$$r_3 = k_3[O_2(g)]^{1/2}\Gamma_{Au^0}{-}CO$$

Step (iv):

$$r_{s2} = k_{s2}\Gamma_{Au^{\delta+}-CO}\Gamma_{O-S}$$

Step (v):

$$r_4 = k_4[O_2(g)]^{1/2}\Gamma_s$$

Step (vi):

$$r_5 = k_5[CO_2(g)]\Gamma_{O-s} - k_{-5}\Gamma_{CO_3^{=}-S}$$

where Γ_i stands for the surface coverage of the I species or surface site; and k_i stands for the kinetic constant of the reaction.

This set of differential equations was numerically integrated (fourth order Runge–Kutta) and the error between the model and the experimental data was minimized with the k_i as parameters (Down-Simplex). Full lines in Fig. 9 represent the best fits of the experimental data with and without CO_2 into the feed. As seen in the figure, this model satisfactorily represents the inhibitory effect of the CO_2 pressure due to the competition for the surface oxygen in the gold-support interphase.

5. Summary and conclusion

The partial and reversible inhibition of the CO oxidation on a well-characterized gold-supported on ceria–zirconia catalyst was investigated using a combination of transient mass spectrometry and in situ infrared spectroscopy. Results showed that this effect cannot by due to structural changes of the catalyst, e.g. sintering of the gold particles, or poisoning by CO or O_2. Instead a correlation was found with the presence of CO_2, incorporated to the reaction feed or produced by the reaction itself. The role of CO_2 in the inhibition of the mechanism of CO oxidation was investigated in detail by means of isotopic transient analysis ($^{13}CO/^{12}CO_2$) monitored by mass spectrometry and by time-resolved and concentration-modulation spectroscopy in DRIFT mode. These results showed that CO adsorbs on neutral (2110 cm^{-1}) and negatively charged gold sites (2060–2020 cm^{-1}). Upon introducing O_2 into the DRIFT cell, $Au^{\delta-}$–CO species are readily oxidized to CO_2, while Au^0–CO species are converted to partially positively charged gold sites, $Au^{\delta+}$–CO, which are then slowly oxidized to CO_2. Moreover, the presence of CO_2 in the gas phase retards the oxidation of $Au^{\delta+}$–CO species. This is ascribed to a competitive adsorption of CO_2 on vacancy sites at the metal–support interphase, producing adsorbed carbonate species and hindering the replenishment of the vacancy by molecular oxygen. This model was validated by simulating the microkinetic mechanism and fitting the temporal evolution of the IR signals of CO-adsorbed species.

Result reported in this work suggest that modification of the support by lowering the CO_2 adsorption, carbonate formation, while maintaining the redox capacity could improve the activity and stability of the gold catalysts for the CO oxidation reaction.

Acknowledgments

We acknowledge the financial support from the Ministry of Education and Science of Spain/FEDER Program of the EU (CSD2009-00013) and Junta de Andalucía (Grant Number P10-FQM-6766) (Groups FQM-110 and FQM-334). SEC and AA thanks to CONICET, ANPCYT and UNL for the financial support.

Appendix A. Supplementary material

Supplementary data associated with this article can be found, in the online version, at http://dx.doi.org/10.1016/j.jcat.2014.05.016.

References

[1] T. Takei, T. Akita, I. Nakamura, T. Fujitani, M. Okumura, K. Okazaki, J. Huang, T. Ishida, M. Haruta, C.G.F.C.J. Bruce, Heterogeneous catalysis by gold, in: Advances in Catalysis, Academic Press, 2013, p. 1 (Chapter 1).
[2] G.C. Bond, C. Louis, D.T. Thompson, Catalysis by Gold, Imperial College Press, London, 2006.
[3] I. Dobrosz-Gómez, I. Kocemba, J. Rynkowski, Catal. Lett. 128 (2009) 297.
[4] E. del Río, G. Blanco, S. Collins, M. Haro, X. Chen, J. Delgado, J. Calvino, S. Bernal, Top. Catal. 54 (2011) 931.
[5] O.H. Laguna, F. Romero Sarria, M.A. Centeno, J.A. Odriozola, J. Catal. 276 (2010) 360.
[6] M. Cargnello, C. Gentilini, T. Montini, E. Fonda, S. Mehraeen, M. Chi, M. Herrera-Collado, N.D. Browning, S. Polizzi, L. Pasquato, P. Fornasiero, Chem. Mater. 22 (2010) 4335.
[7] D. Tibiletti, A. Fonseca, R. Burch, Y. Chen, J. Fisher, A. Goguet, C. Hardacre, P. Hu, D. Thompsett, J. Phys. Chem. B 109 (2005) 22553.
[8] R. Pilasombat, H. Daly, A. Goguet, J.P. Breen, R. Burch, C. Hardacre, D. Thompsett, Catal. Today 180 (2012) 131.
[9] C. Gennequin, M. Lamallem, R. Cousin, S. Siffert, V. Idakiev, T. Tabakova, A. Aboukais, B.L. Su, J. Mater. Sci. 44 (2009) 6654.
[10] G.J. Hutchings, Gold Bull. 42 (2009) 260.
[11] D. Widmann, R. Leppelt, R.J. Behm, J. Catal. 251 (2007) 437.
[12] M. Daté, M. Okumura, S. Tsubota, M. Haruta, Angew. Chem. Int. Ed. 43 (2004) 2129.
[13] M. Haruta, Faraday Discuss. 152 (2011) 11.
[14] I.X. Green, W. Tang, M. Neurock, J.T. Yates, Science 333 (2011) 736.
[15] I.X. Green, W. Tang, M. McEntee, M. Neurock, J.T. Yates, J. Am. Chem. Soc. 134 (2012) 12717.
[16] M. Haruta, Gold Bull. 37 (2004) 27.
[17] G.J. Hutchings, J.K. Edwards, L.J.J.P.W. Roy, Application of gold nanoparticles in catalysis, in: Frontiers of Nanoscience, Elsevier, 2012, p. 249 (Chapter 6).
[18] Y. Hao, M. Mihaylov, E. Ivanova, K. Hadjiivanov, H. Knözinger, B.C. Gates, J. Catal. 261 (2009) 137.
[19] A. Goguet, R. Burch, Y. Chen, C. Hardacre, P. Hu, R.W. Joyner, F.C. Meunier, B.S. Mun, D. Thompsett, D. Tibiletti, J. Phys. Chem. C 111 (2007) 16927.
[20] A. Gomez-Cortes, G. Diaz, R. Zanella, H. Ramirez, P. Santiago, J.M. Saniger, J. Phys. Chem. C 113 (2009) 9710.
[21] P. Konova, A. Naydenov, C. Venkov, D. Mehandjiev, D. Andreeva, T. Tabakova, J. Mol. Catal. A – Chem. 213 (2004) 235.

[22] A.M. Visco, F. Neri, G. Neri, A. Donato, C. Milone, S. Galvagno, Phys. Chem. Chem. Phys. 1 (1999) 2869.
[23] M.C. Raphulu, J. McPherson, E. Lingen, J.A. Anderson, M.S. Scurrell, Gold Bull. 43 (2010) 21.
[24] S. Carrettin, P. Concepción, A. Corma, J.M. López Nieto, V.F. Puntes, Angew. Chem. Int. Ed. 43 (2004) 2538.
[25] T.A. Ntho, J.A. Anderson, M.S. Scurrell, J. Catal. 261 (2009) 94.
[26] J.C. Clark, S. Dai, S.H. Overbury, Catal. Today 126 (2007) 135.
[27] G.Y. Wang, H.L. Lian, W.X. Zhang, D.Z. Jiang, T.H. Wu, Kinet. Catal. 43 (2002) 433.
[28] B.K. Chang, B.W. Jang, S. Dai, S.H. Overbury, J. Catal. 236 (2005) 392.
[29] S.A.C. Carabineiro, A.M.T. Silva, G. Drazic, P.B. Tavares, J.L. Figueiredo, Catal. Today 154 (2010) 293.
[30] M. Daté, M. Haruta, J. Catal. 201 (2001) 221.
[31] F. Vindigni, M. Manzoli, A. Chiorino, F. Boccuzzi, Gold Bull. 42 (2009) 106.
[32] S.E. Collins, J.M. Cies, E. del Rio, M. Lopez-Haro, S. Trasobares, J.J. Calvino, J.M. Pintado, S. Bernal, J. Phys. Chem. C 111 (2007) 14371.
[33] J.M. Cíes, E. del Río, M. López-Haro, J.J. Delgado, G. Blanco, S. Collins, J.J. Calvino, S. Bernal, Angew. Chem. Int. Ed. 49 (2010) 9744.
[34] J.M. Cíes, J.J. Delgado, M. López-Haro, R. Pilasombat, J.A. Pérez-Omil, S. Trasobares, S. Bernal, J.J. Calvino, Chem. Eur. J. 16 (2010) 9536.
[35] M. Lopez-Haro, J.J. Delgado, J.M. Cies, E. del Rio, S. Bernal, R. Burch, M.A. Cauqui, S. Trasobares, J.A. Perez-Omil, P. Bayle-Guillemaud, J.J. Calvino, Angew. Chem. Int. Ed. 49 (2010) 1981.
[36] A. Aguirre, S.E. Collins, Catal. Today 205 (2013) 34.
[37] D. Baurecht, U.P. Fringeli, Rev. Sci. Instrum. 72 (2001) 3782.
[38] T. Tabakova, F. Boccuzzi, M. Manzoli, J.W. Sobczak, V. Idakiev, D. Andreeva, Appl. Catal. A – Gen. 298 (2006) 127.
[39] F. Boccuzzi, A. Chiorino, S. Tsubota, M. Haruta, J. Phys. Chem. 100 (1996) 3625.
[40] M. Chen, D.W. Goodman, Accounts Chem. Res. 39 (2006) 739.
[41] M.S. Chen, D.W. Goodman, Science 306 (2004) 252.
[42] B. Yoon, H. Haakkinen, U. Landman, A.S. Wörz, J.M. Antonietti, S. Abbet, K. Juadai, U. Heiz, Science 307 (2005) 403.
[43] A.S. Worz, U. Heiz, F. Cinquini, G. Pacchioni, J. Phys. Chem. B 109 (2005) 18418.
[44] A. Fielicke, G. VonHelden, G. Meijer, D.B. Pedersen, B. Simard, D.M. Rayner, J. Am. Chem. Soc. 127 (2005) 8416.
[45] J.C. González, J.C. Hernández, M. López-Haro, E. del Río, J.J. Delgado, A.B. Hungría, S. Trasobares, S. Bernal, P.A. Midgley, J.J. Calvino, Angew. Chem. Int. Ed. 121 (2009) 5417.
[46] F. Boccuzzi, A. Chiorino, M. Manzoli, P. Lu, T. Akita, S. Ichikawa, M. Haruta, J. Catal. 202 (2001) 256.
[47] T. Tabakova, F. Boccuzzi, M. Manzoli, D. Andreeva, Appl. Catal. A – Gen. 252 (2003) 385.
[48] H. Noei, A. Birkner, K. Merz, M. Muhler, Y. Wang, J. Phys. Chem. C 116 (2012) 11181.
[49] G. Finos, S. Collins, G. Blanco, E. del Río, J.M. Cíes, S. Bernal, A. Bonivardi, Catal. Today 180 (2012) 9.
[50] C. Binet, M. Daturi, J.-C. Lavalley, Catal. Today 50 (1999) 207.
[51] M. Daturi, C. Binet, J.C. Lavalley, G. Blanchard, Surf. Interface Anal. 30 (2000) 273.
[52] M. Daturi, C. Binet, J.-C. Lavalley, A. Galtayries, R. Sporken, Phys. Chem. Chem. Phys. 1 (1999) 5717.
[53] B. Bachiller-Baeza, I. Rodriguez-Ramos, A. Guerrero-Ruiz, Langmuir 14 (1998) 3556.
[54] K. Pokrovski, K.T. Jung, A.T. Bell, Langmuir 17 (2001) 4297.
[55] A. Simakov, I. Tuzovskaya, A. Pestryakov, N. Bogdanchikova, V. Gurin, M. Avalos, M.H. Farías, Appl. Catal. A – Gen. 331 (2007) 121.
[56] M. Cargnello, V.V.T. Doan-Nguyen, T.R. Gordon, R.E. Diaz, E.A. Stach, R.J. Gorte, P. Fornasiero, C.B. Murray, Science 341 (2013) 771.
[57] S. Carrettin, A. Corma, M. Iglesias, F. Sanchez, Appl. Catal. A – Gen. 291 (2005) 247.
[58] M. Kotobuki, R. Leppelt, D.A. Hansgen, D. Widmann, R.J. Behm, J. Catal. 264 (2009) 67.
[59] M.M. Schubert, A. Venugopal, M.J. Kahlich, V. Plzak, R.J. Behm, J. Catal. 222 (2004) 32.